Applied Catalysis B: Environmental 250 (2019) 89–98

Contents lists available at ScienceDirect

Applied Catalysis B: Environmental

journal homepage: www.elsevier.com/locate/apcatb

Correlation between the H_2 response and its oxidation over TiO_2 and N doped TiO_2 under UV irradiation induced by Fermi level

Kun Wang[a,b], Ting Peng[a,b], Zhongming Wang[a,b], Hong Wang[a,b], Xun Chen[a], Wenxin Dai[a,b,*], Xianzhi Fu[a,*]

[a] Research Institute of Photocatalysis, State Key Laboratory of Photocatalysis on Energy and Environment, Fuzhou University, Fuzhou, 350002, China
[b] Key Laboratory of Eco-materials Advanced Technology (Fuzhou University), Fujian Province University, Fuzhou, 350002, China

ARTICLE INFO

Keywords:
H_2 Photocatalytic oxidation
H_2 Chemisorption
Electron transfer
Photo-assisted gas sensitivity
Fermi level

ABSTRACT

In the previous work, we have ever found that the photocatalytic oxidation of a reactant gas over TiO_2 would be somewhat dependent on the electron transfer behavior between the adsorbed gas and TiO_2 under UV irradiation. To further confirm the viewpoint, in this work, a TiO_2 (in-situ) sample was prepared by an in-situ method, and was tested its gas-sensing performance to H_2 and its photocatalytic performance of oxidizing H_2 as compared to a TiO_2 (commercial) sample. It was found that TiO_2 (in-situ) would increase the conductivity with the introduction of H_2 under UV irradiation, but TiO_2 (commercial) would decrease the conductivity in the same case. Based on the surface structural and electrochemical characteristics of samples, it was proposed that the existence of surface defects over TiO_2 (in-situ) would decrease the Fermi level (E_F), resulting in the electron transfer from the adsorbed H_2 to TiO_2, while the adsorbed H_2 accepted electrons from TiO_2 (commercial) due to its higher E_F. Moreover, the adsorbed H_2 on TiO_2 (in-situ) could be oxidized under UV irradiation but that on TiO_2 (commercial) could be hardly. This indicated that the photocatalytic oxidation of H_2 over TiO_2 would be dependent on the electron transfer direction between the adsorbed H_2 and TiO_2, i.e., the electron-donated H_2 could be oxidized, while the electron-accepted H_2 could be not. This above effect induced by the surface defects could be further demonstrated by a N-doped TiO_2 (N-TiO_2) sample. This N-TiO_2 owned a lower E_F than TiO_2 (in-situ) due to the introduction of a more impurity defects, resulting in a more electron transfer from the adsorbed H_2 to N-TiO_2 and then the oxidation of more H_2. This study also indicated that the adjustment of E_F could improve the photocatalytic activity of oxidizing H_2 by changing the adsorbed behavior of H_2 over TiO_2, which may be applicable for investigating other reactants' oxidation behaviors over other semiconductor photocatalysts.

1. Introduction

As well known, the gas reaction process over a solid catalyst would be somewhat dependent on the adsorption of reactant gases on the catalyst surface. However, when a gas is adsorbed at the surface of a semiconductor catalyst (e.g., transition metal oxide such as TiO_2, ZnO et al.), an electron transfer process can occur between the semiconductor and adsorbate according to the theory of semiconductor adsorbing species (e.g., Boundary layer theory) [1]. For the n-type semiconductor TiO_2, if the surface-state energy level of adsorbate is higher than the Fermi level of TiO_2, the adsorbed species can act as electron donor to donate electrons into TiO_2, resulting in the increase in the surface conductivity of TiO_2. In contrast, if the surface-state energy level of adsorbate is lower than the Fermi level of TiO_2, the adsorbed species (as electron acceptor) can accept the electrons from the conduction band of TiO_2, resulting in the decrease in the surface conductivity of TiO_2. Moreover, the change value in conductivity induced by adsorbing gas can be characterized by a gas sensing property, which can reflect the chemisorption strength of adsorbate (gas) at TiO_2 surface [2]. That is to say, the gas sensing property can partly present the chemisorption behavior (mainly the electron transfer behavior) of the target gas at TiO_2 or other semiconductors, and then have a somewhat relation with the subsequent reaction process of the target gas.

Many works reported that metal oxide sensors could exhibit an excellent gas sensitivity under ultra-violet (UV) /visible light illumination [3–9]. E.g., ZnO [10–12], SnO_2 [4,13] and TiO_2 [14–16] had been widely used in photo-assisted gas sensor for H_2, NO_2, CO and so on. Considering that the probable relation between a reacted gas

* Corresponding authors at: Research Institute of Photocatalysis, State Key Laboratory of Photocatalysis on Energy and Environment, Fuzhou University, Fuzhou, 350002, China.
E-mail addresses: daiwenxin@fzu.edu.cn (W. Dai), xzfu@fzu.edu.cn (X. Fu).

https://doi.org/10.1016/j.apcatb.2019.03.026
Received 31 December 2018; Received in revised form 16 February 2019; Accepted 10 March 2019
Available online 11 March 2019
0926-3373/

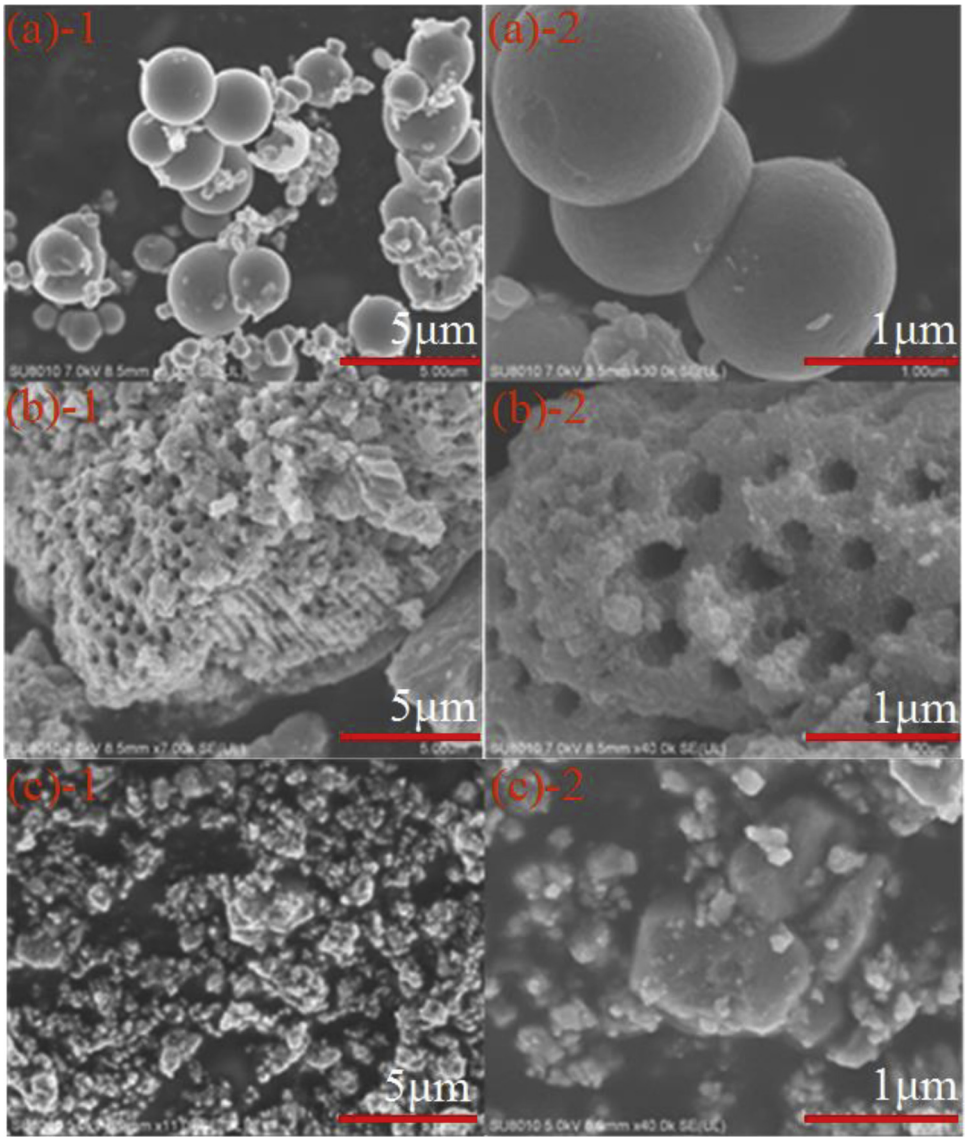

Fig. 1. SEM images of TiO_2 (in-situ) (a-1 and a-2), N-TiO_2 (b-1 and b-2) and TiO_2 (commercial) (c-1 and c-2) sensor samples.

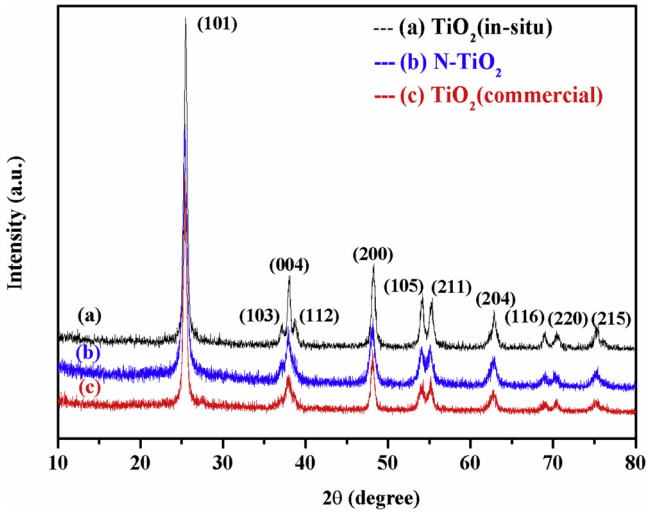

Fig. 2. XRD patterns of TiO_2 (a) TiO_2 (in-situ); (b) N-TiO_2 and (c) TiO_2 (commercial) samples.

Table 1
The textural data of TiO_2 (commercial), N-TiO_2 and TiO_2 (in-situ) samples by N_2 adsorption.

Samples	BET surface area ($m^2 \cdot g^{-1}$)	Pore diameter (nm)	Pore volume ($cm^3 \cdot g^{-1}$)
TiO_2 (commercial)	24.84	4.51	0.054
N-TiO_2	81.51	8.16	0.209
TiO_2 (in-situ)	24.21	4.57	0.053

sensing property and its chemisorption at semiconductor, the photo-assisted gas sensing properties of semiconductors should have a somewhat relation to the photocatalytic reaction of gas over semiconductors. This correlation was also confirmed by our previous works [17,18]. We have ever found that adding polyaniline (PANI) into TiO_2 could enhance the photo-assisted sensing response to CO, which also further promoted the photocatalytic oxidation of CO [17]. Moreover, we also found that the photocatalytic oxidation of CO and H_2 over TiO_2 (prepared by sol-gel method) would be dependent on the electron transfer direction between CO or H_2 and TiO_2 by a photo-assisted gas sensing testing [18]. For CO gas, it could offer electrons to TiO_2, resulting in the decrease in the resistance of TiO_2 sensor under UV irradiation at room

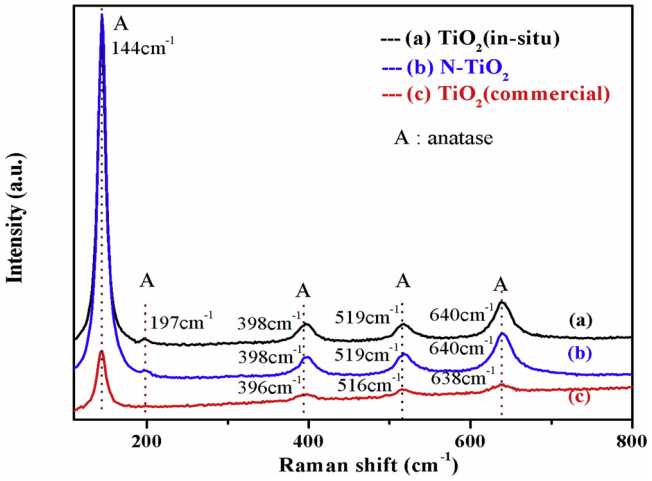

Fig. 3. Raman spectra of different anatase TiO_2 samples: (a) TiO_2 (in-situ), (b) N-TiO_2, (c) TiO_2 (commercial).

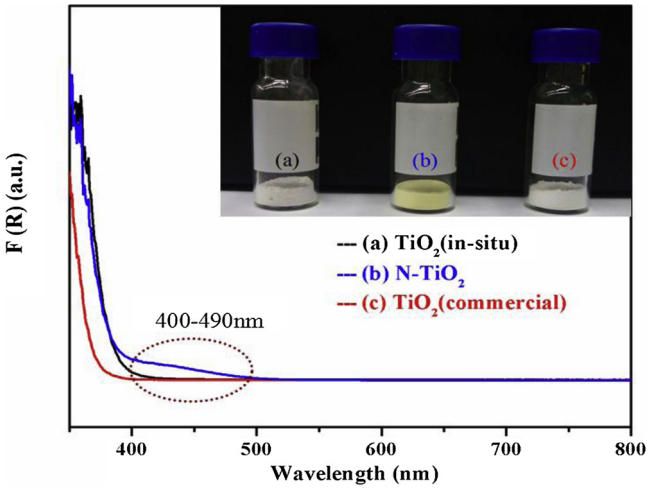

Fig. 4. UV–vis diffuse reflectance spectra (DRS) of (a) TiO_2 (in-situ), (b) N-TiO_2 and (c) TiO_2 (commercial) samples.

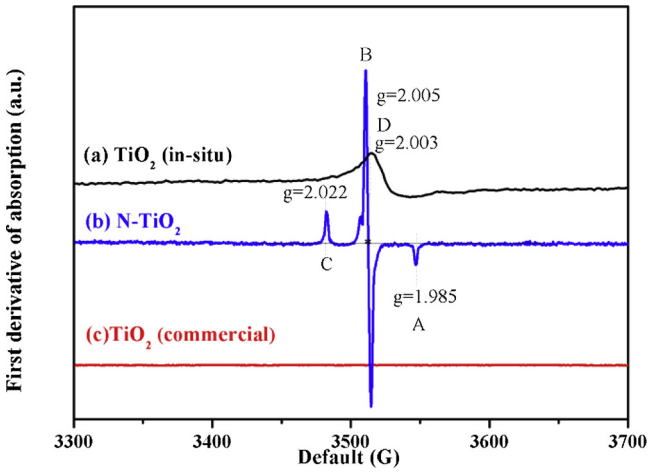

Fig. 5. EPR spectra recorded at room temperature in dark over different samples: (a) TiO_2 (in-situ); (b) N-TiO_2; (c) TiO_2 (commercial). Note that UV light did not cause the apparent change in EPR signals of each sample (the spectra were not shown here).

temperature, and could also be photocatalytic oxidized by this TiO_2 catalyst. In contrast, H_2 gas would accept the electrons from TiO_2, resulting in the increase in the resistance of TiO_2 sensor, but it could not be photocatalytic oxidized. Furthermore, it was proposed that the location of adsorption-state energy level of CO adsorbed at TiO_2 surface was higher than the Fermi level of TiO_2 under UV irradiation, but that of H_2 adsorbed at TiO_2 surface was lower than the Fermi level of TiO_2 in the same case. This study indicated that the Fermi level of TiO_2 would be responsible for the electron transfer direction between the adsorbed gas and TiO_2, and then the photocatalytic oxidation of gas or not. That is to say, adjusting the Fermi level of TiO_2 maybe change the electron transfer direction between the adsorbed reactants and TiO_2, and then change the photocatalytic oxidation behaviors of reactants.

However, the Fermi level of metal oxides is somewhat dependent on its surface state, especially its surface defects [19,20] induced by the process of synthesis [21]. Moreover, the presence of some impurities could also cause the change in Fermi level of TiO_2 [19–21]. E.g., a non-metallic element, such as nitrogen [22–24], carbon [25], sulfur [26,27] and boron [28,29] could adjust the energy gap and the Fermi level of TiO_2. Furthermore, this changed energy gap and the Fermi level could further improve the photocatalytic activity of metal oxides. For example, Anupama et al. [30] have found that doping carbon could modified the band gap of TiO_2 and then promote the photo-degradation of pharmaceutical under visible light irradiation. Adriana et al. [31] have reported that the boron-doped TiO_2 could be excited by visible light and used as effective catalyst in photo-oxidation reactions. In addition, Gyula et al. [32] have also reported that the decrease in the band gap of TiO_2 through N incorporation could facilitate the photolysis of formic acid under visible light irradiation. This above reports showed that different TiO_2 samples may own different Fermi levels due to the presence of different surface defects, which could also be adjusted by doping non-metallic elements.

To further confirm the obtained correlation among the Fermi level of TiO_2, the electron transfer behavior of the adsorbed reactant and its oxidation over TiO_2 under UV irradiation in our previous work [18], in this work, two anatase TiO_2 samples with different Fermi levels were compared their photo-assisted gas sensitivity to H_2 and then their photocatalytic activities of oxidizing H_2. It was expected that a new prepared TiO_2 with a lower Fermi level induced by surface defects maybe accept electrons from the adsorbed H_2 and then photocatalytic oxide H_2 just like that of CO. Moreover, to further lower the Fermi level of TiO_2, nitrogen element was doped into TiO_2 to prepare a N-TiO_2 sample, which also was performed its gas sensing property and photocatalytic activity to H_2. It was found that the decrease in Fermi level of TiO_2-based samples does make the adsorbed H_2 offer electrons to TiO_2 and then be oxidized over TiO_2 under UV irradiation.

2. Materials and methods

2.1. Preparation of TiO_2 sensor

2.1.1. Preparation of commercial-TiO_2 sensor

Commercial-TiO_2 sensor sample was prepared according to our previous work [33]: An interdigitated Au electrode (15 mm × 10 mm, the gap size of 0.15 mm) deposited on the alumina (α-Al_2O_3) substrate was used as the substrate for the gas sensor. The electrode was prepared: A microscope slide (Sail brand, China) was pretreated with acetone, ethanol, and deionized water in sequence, the subsequently dried process (80 °C for 30 min). To prepare the TiO_2 sensor device, a 50 μL TiO_2 suspension (30 mg of commercial TiO_2 powder was dispersed into a 1 mL ethanediol solvent) was dropped onto the clean surface of a comb-like gold electrode. The TiO_2 sensor was dried at 80 °C for 1 h and then calcined in air at 450 °C for 3 h in a tube furnace with a heating rate of 2 °C·min^{-1}. After cooled down to the room temperature naturally, a TiO_2 film sensor device was obtained. In addition, the powder sample obtained from the above TiO_2 film was denoted as TiO_2 (commercial).

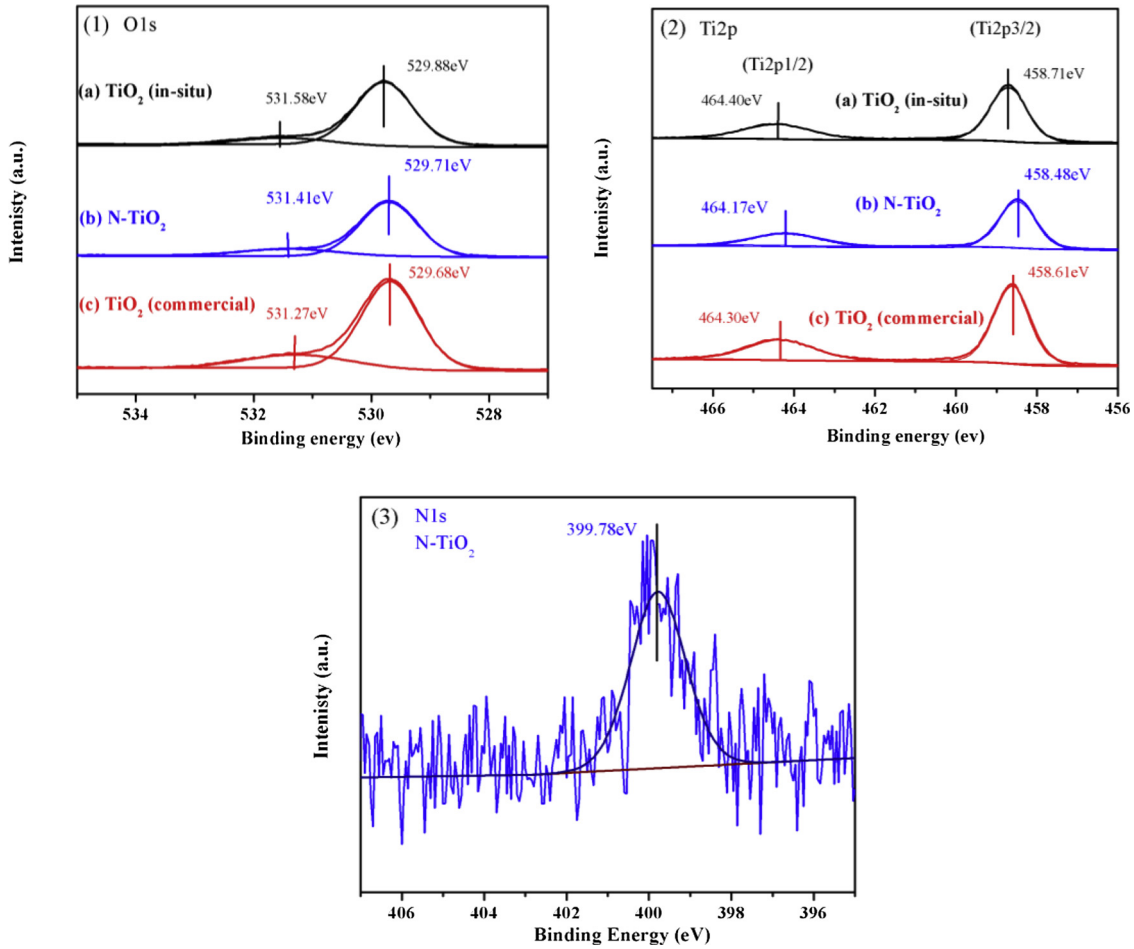

Fig. 6. XPS high-resolution spectra of TiO_2 (in-situ), N-TiO_2 and TiO_2 (commercial) samples: (1) O1s spectra, (2) Ti2p spectra, (3) N1s spectra.

2.1.2. Preparation of TiO_2 sensor by in-situ method

In-situ TiO_2 sensor sample was prepared according to our previous work [33]: An interdigitated Au electrode deposited on the alumina substrate was used as the substrate for the gas sensor. The electrode was first pretreated subsequently with acetone, ethanol, and deionized water, and then treated with piranha solution (30% H_2O_2: 98% H_2SO_4 equivalent to 3:7 v/v) for 3 h in order to increase the surface hydrophilicity of the electrode. After rinsed several times with deionized water and dried in the oven at 80 °C, a clean electrode was obtained. In the second step, the clean electrode was dipped into a precursor solution containing a mixture of titanium isopropoxide and ethanol (1:10 v/v) for 2 min. Then, the electrode was put on a smooth table to rest and be hydrolyzed naturally through the air humidity. Finally, the electrode was calcined at 500 °C for 2 h at a heating rate of 1 °C·min^{-1}, and then let it cool down to room temperature. For characterization and testing purposes, TiO_2 powder sample labeled as TiO_2 (in-situ) was prepared using the above precursor solution, then exposed to air and subsequent hydrolization and calcination processes.

2.1.3. Preparation of N-TiO_2 sensor

N-doped TiO_2 (N-TiO_2) material was prepared by the hydrolysis reaction [34]: a volume of 100 mL ammonia aqueous solution at 30 wt %, supplied by Carlo Erba, was quickly added to 25.0 mL of 97% titanium tetraisopropoxide (TTIP by Sigma Aldrich) during a vigorous stirring of the solution in an ice-bath. After stirring for 1 h, the precipitate was then carefully washed with deionized water and centrifuged to be separated. Then washed precipitates by drying 80 °C were calcined at 450 °C for 30 min to obtain a powder sample, denoted as N-TiO_2 (also used as the photocatalyst) similarly to the process of preparing commercial-TiO_2 sensor in the 2.1.1 section, a N-TiO_2 sensor sample was obtained.

2.2. Characteristics

Surface morphologies of samples were performed with Scanning Electron Microscopy (SEM) (Hitachi S4800). The phase and crystal structure of TiO_2 powder samples were characterized by X-ray diffraction (XRD, D8 Advance, Brucker, Germany) having Cu Kα radiatio (2θ: 10°80°, data analyzed by X'Pert HighScore). Nitrogen isothermal stripping absorption curves of samples were measured at liquid N_2 temperature with a micromeritics ASAP 2020 BET analyzer afterthe sample was outgassed at vacuum and 250 °C for 4 h. The Raman spectrum of the samples were analyzed by Renishaw 2000 in Via confocal Raman spectrometer, the excitation wavelength used was 532 nm Ar^+ laser of 532 nm and scanning scope is 100–800 nm. UV–vis diffuse reflectance spectra (UV–vis DRS) of samples were recorded with UV–vis spectrophotometer (Cary-5000, Varian Co.). X-ray photoelectron spectrometer (XPS) was measured with Mg Kα radiation after monochromatic treatment on the ESCALB mk-ii X-ray photoelectron spectrometer.

Electrochemical testing was used the Metrohm-Autolab AUT302 N Electrochemical workstation, which was conducted in a 3-electrode glass cell using the TiO_2 film as the working electrode, Ag/AgCl (1 M KCl) as the reference electrode, and Pt wire as the counter electrode. The frequency and amplitude were set to 500, 1000 and 1500 Hz and 5 mV, respectively. The Mott-schottky curve was measured in 0.02 mol·L^{-1} Na_2SO_4 solution and tested in dark, in UV light, respectively. The UV light was supplied by a 500 W Xe lamp (also as the light source in other experiments in this work, its spectrogram seen in Fig. S1 in the

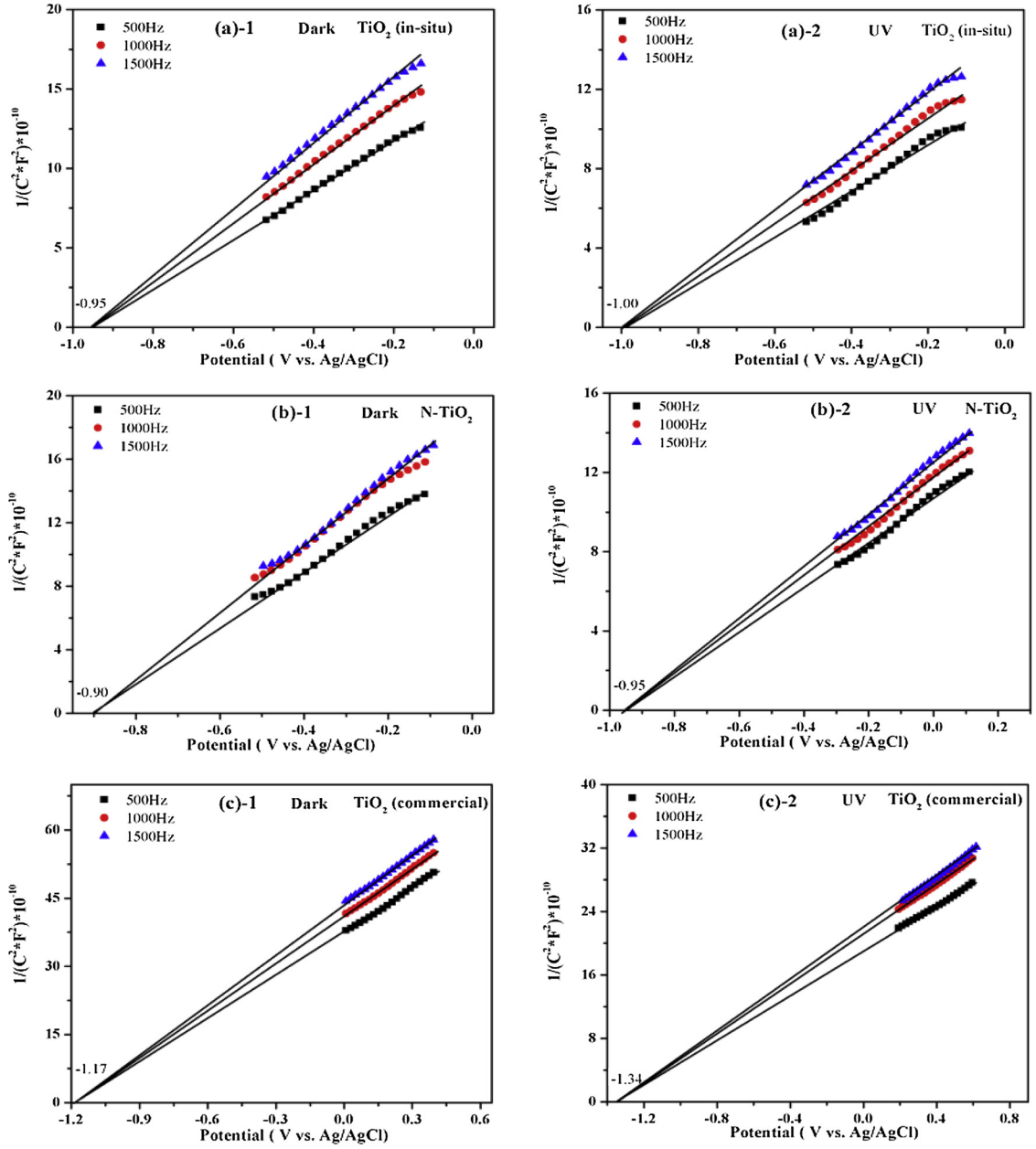

Fig. 7. Mott–Schottky plots (the graph is the point by taking the same number dots of straight lines.): (a)-1 TiO_2 (in-situ) (in dark), (a)-2 TiO_2 (in-situ) (UV); (b)-1 N-TiO_2 (in dark); (b)-2 N-TiO_2 (UV); (c)-1 TiO_2 (commercial) (in dark), (c)-2 TiO_2 (commercial) (UV).

Table 2
The Fermi level values of different samples in dark and under UV irradiation from Fig.7.

Samples	Fermi level value in dark (E_F), V		Fermi level value under UV irradiation (E_F^*), V	
	Vs. Ag/AgCl	Vs. RHE	Vs. Ag/AgCl	Vs. RHE
TiO_2 (commercial)	−1.17	−0.52	−1.34	−0.69
TiO_2 (in-situ)	−0.95	−0.30	−1.00	−0.35
N-TiO_2	−0.90	−0.25	−0.95	−0.30

electrical supporting information (ESI)).

Electron paramagnetic resonance (EPR) spectra were registered at a microwave frequency of 9.8 GHz and power of 6.36 Mw by the Bruker EPR A300 spectrometer and all of the EPR spectra were obtained at room temperature.

2.3. Gas sensing testing

The gas sensing properties of the films were investigated in a chamber of 100 mL, which is made of stainless steel. During the tests, four UV lamps with a wavelength centered at 365 nm (4 W, Philips TL/05) were used as the irradiation source and the total light intensity on the surface of sensing film was 7.3 mW cm^{-2}, a high purity N_2 was introduced into the chamber as the background atmosphere, and H_2 (balance with the high purity N_2) was as the probe gas, and the total flow rate was kept at 250 mL min^{-1}. The film sensor sample was maintained at 200 °C for 1 h in a high purity N_2 before testing (to remove the water and the other gas adsorbates), and then cooled down the room temperature. In addition, the applied voltage was controlled at 8.5 V in testing process. The response of film sensor to the gas was described by the variation of its impedance, and the resistance of the film sensor was measured by a JF02E gas sensing test system (Kunming Gui Yan Jin Feng Tech. Corp. Ltd.) The relative gas sensitivity (S) of the

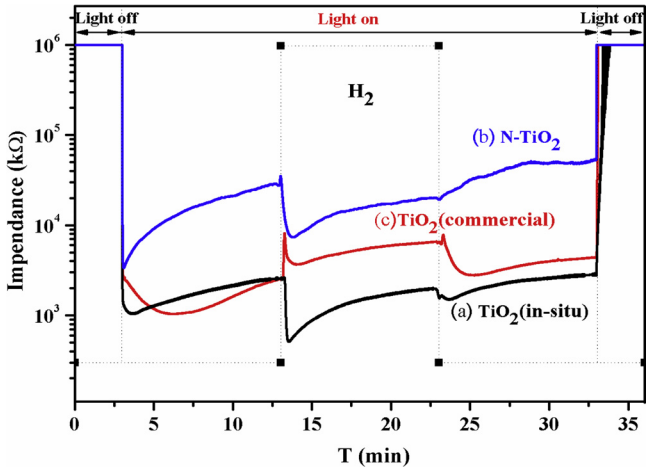

Fig. 8. Gas sensing responses to H_2 under UV light irradiation at room temperature in N_2 atmosphere over different sensor samples: (a) TiO_2 (in-situ); (b) N-TiO_2; (c) TiO_2 (commercial).

Table 3
Gas sensing values of samples to H_2 under UV light at room temperature from the results in Fig. 8.

Sensor samples	R_0 (KΩ)	R_{gas} (KΩ)	$S=\|R_0- R_{gas}\|/R_0$	Electron transfer direction
TiO_2 (in-situ)	2560.89	508.78	0.80	From H_2 to TiO_2
N-TiO_2	34947.41	7384.07	0.79	From H_2 to TiO_2
TiO_2 (commercial)	2513.34	3694.59	0.47	From TiO_2 to H_2

R_0 was assigned to the last impedance value prior to introducing H_2; R_{gas} was assigned to the lowest value after introducing H_2; S was assigned to the gas sensitive response value.

sensor sample was defined as $S=|R_0- R_{gas}|/R_0$, where R_{gas} and R_0 were the impedance measured in the testing gas and in the background atmosphere, respectively.

2.4. Photocatalytic performances

The catalytic oxidation of H_2 over the catalyst sample was conducted in a 50 mL quartz reaction tube. 0.1 g catalyst with a grain size of 0.2–0.3 mm was loaded on the bottom of batch. It was injected reacted gas (including 5 mL high purity of O_2, 2.5 mL high purity of H_2 and 42.5 mL He) after vacuuming the tube (to let the reaction gases spread more easily). Placed the tube in dark for 10 min to reach a balance, and extracted the 1 mL gas in tube for analyzing contents. Then kept the tube in dark for 50 min, and tested the H_2 and O_2 contents. Finally, the reaction tube was illuminated with UV light for 1 h, and tested the reactants contents again. The reacted gases contents were analyzed using an offline gas chromatograph system equipped with a thermal conductivity detector and a flame ionization detector (Agilent 7890D, Porapark R). Here, since the formed H_2O by H_2 oxidation product may be adsorbed at the sample surface, the catalytic activity was evaluated by the decrease of H_2 content.

3. Results and discussion

3.1. The properties of powder samples

Fig. 1 shows the surface morphology of TiO_2 (commercial), TiO_2 (in-situ) and N-TiO_2 samples. It was found that the nanoparticle size of both TiO_2 (in-situ) (a-1 and a-2) and N-TiO_2 (b-1 and b-2) was larger than that of TiO_2 (commercial) (c-1 and c-2). Moreover, TiO_2 (in-situ) sample was mainly consist of a stacked structure by a number of smooth spherical shape nanoparticles with different sizes, while N-TiO_2 sample exhibited an orderly macroporous channel. However, TiO_2 (commercial) sample was made up irregular shape of nanoparticles.

Fig. 2 shows the XRD pattern of TiO_2 (in-situ), N-TiO_2 and TiO_2 (commercial) samples. All samples exhibited diffraction peaks at $2\theta = 25.4°$, 37.8°, 48.1°, 54.0°, 55.1°, 62.8°, 68.8°, 72.3° and 75.1°, which could be corresponded to (101), (004), (200), (105), (211), (204), (116), (220) and (215) crystal planes of anatase TiO_2 (JPCDS No. 21–1272). As compared to TiO_2 (commercial) sample, both TiO_2 (in-situ) and N-TiO_2 samples exhibited another two small peaks at 36.9° and 38.6°, indexed respectively to (103) and (112) crystal planes of anatase TiO_2 (but the two peaks in N-TiO_2 were weaker than those in TiO_2 (in-situ), respectively), indicating that the two kinds of crystal planes were exposed to the surface of both TiO_2 (in-situ) and N-TiO_2 samples [35,36]. Moreover, the (103) and (112) crystal planes, generally induced by surface defects, was also observed in the HR-TEM images of TiO_2 (in-situ) and N-TiO_2 samples (seeing Fig. S2 in ESI). In addition, N-TiO_2 samples exhibited a stronger peak (a smaller peak width at half height) than both TiO_2 (in-situ) and TiO_2 (commercial) samples, indicating that the former owned a larger crystallite size than the two latter according to the Scherrer formula [37]. This difference also led to the different textual structure of N-TiO_2 from that of TiO_2 (in-situ) or TiO_2 (commercial) (seeing Fig. S3 in ESI). As shown in Table 1, TiO_2(in-situ) owned a surface area similar to that of TiO_2 (commercial), but less than that of N-TiO_2.

For anatase TiO_2, the Raman spectra generally exhibited the major Raman bands at 144, 197, 399, 515, 519, and 639 cm^{-1}, which could be assigned as six Raman-active modes of anatase phase with the symmetries of Eg, Eg, B1g, A1g, B1g and Eg, respectively [38]. Fig. 3 shows the Raman spectra of TiO_2 (in-situ), N-TiO_2 and TiO_2 (commercial) powder samples. As can be seen, TiO_2 (commercial) sample displayed four peaks at 144 (Eg), 396 (B1g), 516 (A1g), and 638 cm^{-1} (Eg), while both TiO_2 (in-situ) and N-TiO_2 samples exhibited a tiny shift of four peaks (from 396, 516 and 638 cm^{-1} to 398, 519 and 640 cm^{-1}, respectively) as compared to the former. This shift in frequency could be attributed to the interpretation of non-stoichiometry in TiO_2 crystal structure induced by the oxygen vacancies or the disorder of some phases [39], indicating that TiO_2 (in-situ) and N-TiO_2 samples owned more deficiencies than TiO_2 (commercial) sample, consistent with the XRD result in Fig. 2. In addition, another peak at 197 cm^{-1}, also attributed to the Eg of anatase phase, appeared over TiO_2 (in-situ) and N-TiO_2 samples, indicating that some lattice may be exposed to the sample surface.

Fig. 4 shows the UV–vis diffuse reflectance spectra of three samples. As compared to the white TiO_2 (commercial) sample, the white TiO_2 (in-situ) and the faint yellow N-TiO_2 sample exhibited a red-shifted

Table 4
The results of catalytically oxidizing H_2 over three samples under UV irradiation at room temperature.

Samples	The initial concentration of H_2 (ppm)	The concentration of H_2 in dark for 1 h (ppm)	The concentration of H_2 under UV light for 1 h (ppm)	Characteristic
TiO_2 (in-situ)	34741.7	33917.9	26833.0	[a]H_2 oxidized
N-TiO_2	29539.8	27868.7	18665.4	[a]H_2 oxidized
TiO_2 (commercial)	32858.7	31305.2	30881.5	H_2 not oxidized

a- O_2 contents (not shown here) also decreased, indicating that H_2 was oxidized by O_2.

Table 5
Correlation between H_2 sensing response and its oxidation over three samples under UV irradiation.

Samples	Fermi level value (V) under UV irradiation	Electron transfer direction	H_2 oxidation under UV irradiation
TiO_2 (in-situ)	−1.00	From H_2 to TiO_2	Yes
N-TiO_2	−0.95	From H_2 to N-TiO_2	Yes
TiO_2 (commercial)	−1.34	From TiO_2 to H_2	No

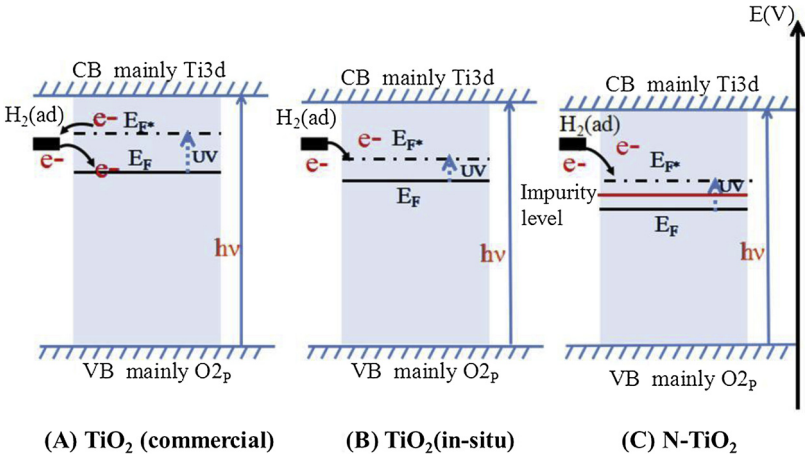

Fig. 9. The proposed process of electron transfer over TiO_2 (commercial), TiO_2 (in-situ) and N-TiO_2 samples adsorbing H_2. Here, electrons transferring from TiO_2 (commercial) to the adsorbed H_2 (H_2 (ad)) due to a higher E_F^*, while electrons transferring from H_2 (ad) to TiO_2 (in-situ) or N-TiO_2 due to a lower E_F^*.

band gap absorption (from 366 nm (3.39 eV) to 384 nm (3.23 eV) and 386 nm (3.21 eV), respectively). In addition, N-TiO_2 exhibited an obviously stronger absorption in the range from 400 m to 490 nm, indicating that N-TiO_2 owned an absorption in visible region [40]. This red shift in band gap absorption for TiO_2(in-situ) and N-TiO_2 samples could be attributed to the existed defect level or impurity level.

Fig. 5 shows the EPR spectra of TiO_2 (commercial), TiO_2 (in-situ) and N-TiO_2 samples at room temperature without UV light. As can be seen, N-TiO_2 sample exhibited a triplet g value sharp signals at g = 1.985, 2.005 and 2.022, respectively. Here, the peak at g = 1.985 could be assigned to the surface Ti^{3+}, probably induced by the surface Ti^{4+} accepting electrons from the rich-electron nitrogen element. The peak at g = 2.005 could be assigned to the oxygen vacancies with single electron, indicating that N-TiO_2 owned a lot of oxygen vacancies (consistent with the Raman result in Fig. 3). In addition, the adsorbed O_2 at Ti^{4+} cations could also capture electrons to form the O_2^- radical ions (corresponding to the peak at g = 2.022) [41–43]. These results indicated that the N-TiO_2 sample with oxygen vacancies, could effectively inhibit the combination of electron and hole, resulting in the promoted electron migration [43] and then a strong EPR signal (forming a more single electron species). Similarly to N-TiO_2, the TiO_2 (in-situ) sample also exhibited a weak at g = 2.003, indicating the existence of oxygen vacancies. However, another two peaks at g = 2.022 and g = 1.985 were not observed for TiO_2 (in-situ), meaning that maybe only a tiny oxygen vacancies existed at the sample surface.

The surface composition and chemical state of samples could be also identified by XPS analysis. As shown in Fig. 6–(1), the O1s spectra of TiO_2 (commercial), TiO_2 (in-situ) and N-TiO_2 samples appeared two peaks respectively. For TiO_2 (commercial), the lower peak at 529.68 eV for O1s assigned to the typical lattice oxygen (Ti-O), and the higher peak at 531.27 eV ascribed to the surface hydroxyl (Ti-O-H) of TiO_2 [44]. However, the binding energy (BE) values of O1s for the lattice oxygen of TiO_2 (in-situ) sample exhibited a positive shift from 529.68–529.88 eV, and that of the surface hydroxyl groups shifted from 531.27–531.58 eV as compared to the TiO_2 (commercial) sample, indicating that the electron density of the oxygen species of TiO_2 (in-situ) was lower than that of TiO_2 (commercial), which may be caused by the oxygen vacancies. In addition, as for N-TiO_2, the BE values of oxygen species also presented a positive shift (from 529.68–529.71 eV for the lattice oxygen and from 531.27–531.41 eV for the surface hydroxyl groups, respectively). This also indicated that the electron density of the oxygen species in N-TiO_2 was reduced due to the existence of surface defects by doping nitrogen.

Fig. 6-(2) shows the Ti2p high-resolution spectra of TiO_2 (commercial), TiO_2 (in-situ) and N-TiO_2 samples As compared to that of TiO_2 (commercial) ($Ti2p_{3/2}$ at 458.61 eV, $Ti2p_{1/2}$ at 464.30 eV), the BE values of $Ti2p_{3/2}$ (458.71 eV) and $Ti2p_{1/2}$ (464.40 eV) of TiO_2 (in-situ) exhibited a positive shift of ca. 0.1 eV, indicating that TiO_2 (in-situ) owned a higher electron density at Ti sites. However, N-TiO_2 exhibited a negative shift at BE of $Ti2p_{3/2}$ (from 458.61 to 458.48 eV) and $Ti2p_{1/2}$ (from 464.30 to 464.17 eV) as compared to TiO_2 (commercial) indicating that the electron density of Ti at N-TiO_2 surface was increased, which may be caused by the doping of rich-electron nitrogen element. Note that no peak of Ti^{3+} appeared over N-TiO_2 (maybe the amount of Ti^{3+} too few), although the result of EPR in Fig. 5 showed the existence of Ti^{3+} in N-TiO_2. In addition, the BE of N1s at 399.78 eV for N-TiO_2 sample in Fig. 6-(3) could be attributed to the anionic N– in O-Ti-N linkages [35,36,45,46], indicating that nitrogen was doped into the lattice of TiO_2.

3.2. Mott–Schottky plots of powder samples

The above results of Raman, EPR and XPS showed that N-TiO_2 and TiO_2 (in-situ) samples owned more surface defects. These defects maybe bring down the Fermi level of TiO_2. To confirm it, a series of Mott–Schottky plots of three samples were tested.

Fig. 7 exhibits the Mott–Schottky plots of TiO_2 (commercial), TiO_2 (in-situ) and N-TiO_2 samples in dark or under UV irradiation, respectively. Since the conduction band position of a n-type semiconductor is very close to the flat band potential [47,48], here the obtained flat band potential in Fig. 7 could be regarded as the Fermi level (E_F) of sample.

As seen in Fig. 7, the flat-band potential (corresponding to E_F) with respect to Ag/AgCl (1 M KCl) electrode could be measured by different frequencies (500, 1000 and 1500 Hz) of Mott–Schottky plots. The flat-

band potentials of TiO_2 (commercial), TiO_2 (in-situ) and N-TiO_2 in dark were -1.17, -0.95 and -0.90 V, respectively. Apparently, N-TiO_2 exhibited the lowest E_F value, in accordance with its owning the most amount of surface defects, indicating that the existence of surface defects did really put down the flat-band potential (E_F). However, under UV light irradiation, the flat-band potential value (of TiO_2 (commercial), TiO_2 (in-situ) and N-TiO_2 went up to -1.34, -1.00 and -0.95 V, respectively, indicating that the light-excited electron transition behavior could elevate the E_F value of each sample (Strictly speaking, the non-equilibrium (transient equilibrium) replacement of the Fermi level in UV light is called the quasi-Fermi level E_F^* [49]). In fact, it has been reported that the Fermi level was dependent on the electron accumulation within the semiconductor particles, the Fermi level becomes more negative and shifts closer to the conduction band edge by the more electrons accumulation [50,51]. T. Berger et al. also reported that the Fermi level of anatase TiO_2 nanoparticles could be controlled by the electron accumulation in the TiO_2 electrode in an electrochemical cell under a certain set of conditions [52]. Note that the increase in E_F of TiO_2 (in-situ) (from -0.95 V to -1.0 V) or N-TiO_2 (from -0.90 to -0.95 V) was much less than that of TiO_2 (commercial) (from -1.17 to -1.34 V). This maybe because the excited electrons could be captured by surface defects, resulting in the decrease of electrons in conducting band and then a little increase of E_F [53].

Furthermore, the above the flat-band potential (E_F) could be converted to the potential value reference to the reversible hydrogen electrode (RHE) by the following equation [54]:

$$ERHE = EAg/AgCl + 0.059pH + E^{\theta}Ag/AgCl(1MKCl)$$

where, $E^{\theta}_{Ag/AgCl}$ (1 M KCl) = 0.236 V at 25 °C. According to this equation, the E_F value (vs. RHE) of TiO_2 (commercial), TiO_2 (in-situ) and N-TiO_2 in Fig. 7 was -0.52 V, -0.30 V, -0.25 V in dark and -0.69 V, -0.35 V, -0.30 V under UV irradiation, respectively (seeing Table 2). This result was also in accordance with the value calculated by electronegativity concept [55,56]. As compared to TiO_2 (commercial), N-TiO_2 sample exhibited a lower conduction band due to its higher electronegativity.

In addition, the UPS result showed that the work function value of TiO_2 (commercial), TiO_2 (in-situ) and N-TiO_2 samples was 3.0, 3.62 and 3.80 eV, respectively (seeing Fig. S4 in ESI), also indicating that both TiO_2 (in-situ) and N-TiO_2 samples owned a lower Fermi level than TiO_2 (commercial).

3.3. Gas sensing responses of sensor samples

Fig. 8 shows the gas sensing responses of TiO_2 (in-situ), N-TiO_2 and TiO_2 (commercial) sensor samples to H_2 under UV light irradiation at room temperature in N_2 atmosphere. The impedances of three samples decreased rapidly with the introduction of UV light, due to the production of the photo-generated electrons. With the increase of time, the impedances of three samples would increase slowly, which could be attributed to the change in the surface state of TiO_2 or N-TiO_2 induced by UV light. Here, the generation of electrons, the recombination of electrons by holes, the capture of electrons by defects or surface hydroxyls, and the electrons transfer would make some changes with the duration of introducing UV light, especially under the bias voltage [35]. When H_2 was introduced into the testing system, the impedances of both TiO_2 (in-situ) and N-TiO_2 samples decreased primarily, and then increased slowly (but the final value was lower than the initial value). However, the impedance of TiO_2 (commercial) sample increased integrally. This indicated that the absorbed H_2 on TiO_2 (in-situ) or N-TiO_2 surface, would offer electrons to the semiconductor, but that on TiO_2 (commercial) would accept electrons from semiconductor [33].

Further comparing the gas sensitivity values (S) of three sensor samples to H_2 (seeing Table 3), it can be seen that both TiO_2 (in-situ) and N-TiO_2 samples exhibited a higher value of gas sensitivity (S = 0.79 for N-TiO_2, and S = 0.80 for TiO_2 (in-situ)) than the TiO_2 (commercial) sample (S = 0.47), indicating that both TiO_2 (in-situ) and N-TiO_2 could also promote H_2 gas sensitivity as compared to the TiO_2 (commercial) sample. This difference may be ascribed to the difference in Fermi level of three samples.

3.4. Photocatalytic activities of powder samples

In our previous work [18], we have found that the electron-donated CO could be oxidized but the electron-accepted H_2 not be oxidized over a TiO_2 catalyst under UV irradiation. However, in this work, the H_2 would act as electron donor when it was adsorbed on TiO_2 (in-situ) and N-TiO_2 samples. According to the above viewpoint, this electron-donated H_2 would be photocatalytically oxidized just like that the electron-donated CO. To confirm it, the photocatalytic performances of oxidizing H_2 over three samples were tested under UV irradiation.

Table 4 shows the change of H_2 concentration in an intermittent reactor (quartz tube) over three catalyst samples in dark and under UV irradiation. After 1 h in dark, the H_2 concentration over all three samples would decrease slightly due to the adsorption of H_2. However, adding UV light would cause different extents of change in H_2 concentration over different samples. The H_2 concentration almost kept unchanged (just a tiny decrease) over TiO_2 (commercial) under UV irradiation for 1 h but would decrease obviously over TiO_2 (in-situ) and N-TiO_2 in the same case. This result indicated that both TiO_2 (in-situ) and N-TiO_2 could catalytically oxidize H_2 under UV irradiation, but TiO_2 (commercial) hardly did it. This further confirmed the viewpoint in our previous work [18].

4. Proposed process of electron transfer over TiO_2 or N-TiO_2 absorbing H_2

Based on the above results of Fermi level, photo-assisted gas sensing response and photocatalytic performances of three samples (seeing Table 5), it was found that H_2 photocatalytic oxidation over TiO_2 (in-situ), N-TiO_2 and TiO_2 (commercial) samples was actually dependent on the electron transfer behavior between the adsorbed H_2 and the sample surface. As H_2 was adsorbed on TiO_2 (in-situ) and N-TiO_2 under UV irradiation, it donated electrons into TiO_2 and then was oxidized by O_2, while H_2 was adsorbed on TiO_2 (commercial) under UV irradiation, it accepted electrons from TiO_2 and could not be oxidized. In other words, the pre-oxidized H_2 (donating electrons, H_2^+) was easily oxidized by O_2 as compared to the pre-reduced H_2 (accepting electrons, H_2^-) over TiO_2 under UV irradiation.

Furthermore, according to the boundary layer theory of semiconductor adsorbing gas [1] and our previous work [18], this different electron transfer behavior between the adsorbed H_2 and semiconductor maybe depended on the Fermi level of semiconductor itself. For TiO_2 (commercial), the adsorbed H_2 (H_2(ad)) usually offer electrons to TiO_2 due to its low E_F in dark (seeing Fig. 9A). However, UV irradiation could elevate the Fermi level (i.e., E_F*) of TiO_2 (even higher than the adsorption-state energy level of H_2), resulting in the electron transfer from TiO_2 (commercial) to the H_2(ad) under UV irradiation. However, TiO_2 (in-situ) owned a low E_F or E_F* value (lower than the adsorption-state energy level of H_2) due to the existed surface defects, the electrons would transfer from the H_2(ad) to TiO_2 (in-situ) under UV irradiation (seeing Fig. 9B). For N-TiO_2, the existed impurity level induced by N doping would further push down the Fermi level (E_F and E_F*) [53,57], resulting in the adsorbed H_2 also donating electrons into N-TiO_2 under UV irradiation (seeing Fig. 9C).

This above result also shows, although H_2 can be thermodynamically oxidized by O_2 over all three samples (the valence band level of each sample was lower than the standard reduction potential of half reaction ($H_2 + 2e \rightarrow 2H^+$), while its conductive band level was higher than the standard reduction potential of other half reaction ($1/2O_2 + 2H^+ + 2e \rightarrow H_2O$) [18], its oxidation would be actually dependent on the electron transfer behavior when it was adsorbed at each sample, which further controlled by the sample's Fermi level. That is to

say, H_2 oxidation over a semiconductor not only depends on its valence band level (thermodynamic controlling), but also depends its conducting band level (near to the Fermi level) (dynamic controlling). This viewpoint may be applicable for understanding other reactant's photocatalytic oxidation behaviors over other semiconductors.

5. Conclusions

From the present investigation the following conclusions can be drawn:

(I) H_2 oxidation over three TiO_2-based samples under UV irradiation was dependent on the photo-assisted H_2 sensing response behavior over each sample, i.e., H_2 photocatalytic oxidation behavior over TiO_2-based semiconductor was dependent on the electron transfer direction between the adsorbed H_2 and semiconductor under UV irradiation: The adsorbed H_2 over TiO_2 (commercial) acted as an electron acceptor (electrons transfer from semiconductor to H_2) and then could not be oxidized, but that at TiO_2 (in-situ) or N-TiO_2 acted as an electron donor (electrons transfer from H_2 to semiconductor) and then was oxidized.

(II) The electron transfer direction between H_2 and semiconductor sample was dependent on the Fermi level of sample: The Fermi level of TiO_2 (in-situ) or N-TiO_2 was lower than that of TiO_2 (commercial) in dark and UV light, respectively, resulting in electron transfer from H_2 to the two former samples but from the latter sample to H_2.

(III) The Fermi level of each sample was somewhat dependent on its surface defects: Both TiO_2 (in-situ) and N-TiO_2 owned a more exposed lattice plane and oxygen vacancies as compared to TiO_2 (commercial), resulting in the Fermi level of two former samples lower than that of the latter sample.

Acknowledgments

This work was financially supported by the National Natural Science Foundation of China (nos. 21273037 and 21872030) and the Science & Technology Plan Project of Fujian Province (no.2014Y2003).

Appendix A. Supplementary data

Supplementary material related to this article can be found, in the online version, at doi:https://doi.org/10.1016/j.apcatb.2019.03.026.

References

[1] S.R. Morrison, The Chemical Physics of Surface, Plenum, N.Y, 1977.
[2] W. Göpel, G. Rocker, Phys. Rev. B 28 (1983) 3427–3438.
[3] Y. Yao, M.L. Yin, J.Q. Yan, D. Yang, S.Z. (Frank) Liu, Controllable synthesis of Ag-WO_3 core-shell nanospheres for light-enhanced gas sensors, Sens. Actuators B 251 (2017) 583–589.
[4] T. Hyodo, K. Urata, K. Kamada, T. Ueda, Y. Shimizu, Semiconductor-type SnO_2-based NO_2 sensors operated at room temperature under UV-light irradiation, Sens. Actuators B 253 (2017) 630–640.
[5] H.Y. Li, Z.X. Cai, J.C. Ding, X. Guo, Gigantically enhanced NO sensing properties of WO_3/SnO_2 double layer sensors with Pd decoration, Sens. Actuators B 220 (2015) 398–405.
[6] M. Trawka, J. Smulko, L. Hasse, C.G. Granqvist, F.E. Annanouch, R. Ionescu, Fluctuation enhanced gas sensing with WO_3 based nanoparticle gas sensors modulated by UV light at selected wavelengths, Sens. Actuators B 234 (2016) 453–461.
[7] E. Wongrat, N. Chanlek, C. Chueaiarrom, B. Samransuksamer, N. Hongsith, S. Choopun, Low temperature ethanol response enhancement of ZnO nanostructures sensor decorated with gold nanoparticles exposed to UV illumination, Sens. Actuators A 251 (2016) 188–197.
[8] E. Comini, G. Sberveglieri, M. Ferroni, V. Guidi, G. Martinelli, Response to ethanol of thin films based on Mo and Ti oxides deposited by sputtering, Sens. Actuators B 93 (2003) 409–415.
[9] Z. Zhu, J.L. Chang, R.J. Wu, Fast ozone detection by using a core-shell Au@TiO_2 sensor at room temperature, Sens. Actuators B Chem. 214 (2015) 56–62.
[10] B. Gong, T.L. Shi, W. Zhu, G.L. Liao, X.P. Li, J. Huang, T.Y. Zhou, Z.R. Tang, UV irradiation-assisted ethanol detection operated by the gas sensor based on ZnO nanowires/optical fiber hybrid structure, Sens. Actuators B 245 (2017) 821–827.
[11] L.X. Meng, Q. Xu, Z. Sun, G.D. Li, S. Bai, Z.H. Wang, Y. Qin, Enhancing the performance of room temperature ZnO microwire gas sensor through a combined technology of surface etching and UV illumination, Mater. Lett. 212 (2018) 296–298.
[12] Q. Geng, Z.J. He, X. Chen, W.X. Dai, X.X. Wang, Gas sensing property of ZnO under visible light irradiation at room temperature, Sens. Actuators B 188 (2013) 293–297.
[13] T.M. Li, W. Zeng, D.F. Shi, S. Hussain, UV-enhanced hydrogen sensor based on nanocone-assembled 3D SnO_2 at low temperature, Mater. Lett. 161 (2015) 648–651.
[14] A. Nikfarjama, N. Salehifar, Improvement in gas-sensing properties of TiO_2 nanofiber sensor by UV irradiation, Sens. Actuators B 211 (2015) 146–156.
[15] Z.M. Wang, K. Wang, X.Y. Peng, Q. Geng, X. Chen, W.X. Dai, X.Z. Fu, X.X. Wang, Comparative study of ultraviolet light and visible light on the photo-assisted conductivity and gas sensing property of TiO_2, Sens. Actuators B 248 (2017) 724–732.
[16] Q. Geng, X.H. Lin, R.R. Si, X. Chen, W.X. Dai, X.Z. Fu, X.X. Wang, The correlation between the ethylene response and its oxidation over TiO_2 under UV irradiation, Sens. Actuators B Chem. 174 (2012) 449–457.
[17] Z.M. Wang, X.Y. Peng, C.Y. Huang, X. Chen, W.X. Dai, X.Z. Fu, CO gas sensitivity and its oxidation over TiO_2 modified by PANI under UV irradiation at room temperature, Appl. Catal. B: Environ. 219 (2017) 379–390.
[18] X.Y. Peng, Z.J. He, K. Yang, X. Chen, X.X. Wang, W.X. Dai, X.Z. Fu, Correlation between donating or accepting electron behavior of the adsorbed CO or H_2 and its oxidation over TiO_2 under ultraviolet light irradiation, Appl. Surf. Sci. 360 (2016) 698–706.
[19] V.N. Brudnyi, S.N. Grinyaev, V.E. Stepanov, Local neutrality conception: fermi level pinning in defective semiconductors, Physical B 212 (1995) 429–435.
[20] V.N. Brudnyi, S.N. Grinyaev, N.G. Kolin, A model for Fermi-level pinningin semiconductors: radiation defects, interface boundaries, Physical B 348 (2004) 213–225.
[21] S.A. Gao, A.P. Xian, L.H. Cao, R.C. Xie, J.K. Shang, Influence of calcining temperature on photo response of TiO_2 film under nitrogen and oxygen in room temperature, Sens. Actuators B 134 (2008) 718–726.
[22] C. Chen, H. Bai, S. Chang, C. Chang, W. Den, Preparation of N-doped TiO_2 photocatalyst by atmospheric pressure plasma process for VOCs decomposition under UV and visible light sources, J. Nanoparticle Res. 9 (2007) 365–375.
[23] H. Irie, Y. Watanabe, K. Hashimoto, Nitrogen-concentration dependence on photocatalytic activity of $TiO_{2-x}Nx$ powders, J. Phys. Chem. B 107 (2003) 5483–5486.
[24] R. Asahi, T. Morikawa, T. Ohwaki, K. Aoki, Y. Taga, Visible-light photocatalysis in nitrogen-doped titanium oxides, Science 93 (2001) 269–271.
[25] B.L. Yan, J. Zhou, X.Y. Liang, K.N. Song, X.T. Su, Facile synthesis of flake-like TiO_2/C nano-composites for photocatalytic H_2 evolution under visible-light irradiation, Appl. Surf. Sci. 392 (2017) 889–896.
[26] M. Katoh, H. Aihara, T. Horikawa, T.H. Tomida, Spectroscopic study for photocatalytic decomposition of organic compounds on titanium dioxide containing sulfur under visible light irradiation, J. Colloid Interface Sci. 298 (2006) 805–809.
[27] T. Umebayashi, T. Yamaki, S. Tanaka, K. Asai, Visible light-induced degradation of methylene blue on S-doped TiO_2, Chem. Lett. 32 (2003) 330–331.
[28] X.N. Lu, B.Z. Tian, J.L. Zhang, Preparation of boron-doped TiO_2 films by autoclaved-sol method at low temperature and study on their photocatalytic activity, Thin Solid Films 519 (2010) 111–116.
[29] D.M. Chen, D. Yang, Q. Wang, Z.Y. Jiang, Effects of boron doping on photocatalytic activity and microstructure of titanium dioxide nanoparticles, Ind. Eng. Chem. Res. 45 (2006) 4110–4116.
[30] A. Surenjan, B. Sambandam, T. Pradeep, L. Philip, Synthesis, characterization and performance of visible light active C-TiO_2 for pharmaceutical photo degradation, J. Environ. Chem. Eng. 5 (2017) 757–767.
[31] A. Zaleska, J.W. Sobczak, E. Grabowska, J. Hupka, Preparation and photocatalytic activity of boron-modified TiO_2 under UV and visible light, Appl. Catal. B: Environ. 78 (2008) 92–100.
[32] G. Halasi, G. Schubert, F. Solymosi, Photodecomposition of formic acid on N-doped and metal promoted TiO_2 production of CO-Free H_2, J. Phys. Chem. C 116 (2012) 15396–15405.
[33] X.Y. Peng, Z.M. Wang, P. Huang, X. Chen, X.Z. Fu, W.X. Dai, Comparative study of two different TiO_2 film sensors on response to H_2 under UV light and room, Sensors 16 (2016) 1249.
[34] V. Vaiano, O. Sacco, D. Sannino, P. Ciambelli, Photocatalytic removal of spiramycin from wastewater under visible light with N-doped TiO_2 photocatalysts, Chem. Eng. J. 261 (2015) 3–8.
[35] Y. Cong, J.L. Zhang, F. Chen, M. Anpo, Synthesis and characterization of nitrogen-doped TiO_2 nanophotocatalyst with high visible light activity, J. Phys. Chem. C 111 (2007) 6976–6982.
[36] J. Wang, D.N. Tafen, J.P. Lewis, Z.L. Hong, A. Manivannan, M.J. Zhi, M. Li, N.Q. Wu, Origin of photocatalytic activity of nitrogen-doped TiO_2 nanobelts, J. Am. Chem. Soc. 131 (2009) 12290–12297.
[37] C.P. Kumar, N.O. Gopal, T.C. Wang, M.S. Wong, S.C. Ke, EPR investigation of TiO_2 nanoparticles with temperature dependent properties, J. Phys. Chem. B 110 (2006) 5223–5229.
[38] J. Zhang, M.J. Li, Z.C. Feng, J. Chen, C. Li, UV Raman spectroscopic study on TiO_2. I. Phase transformation at the surface and in the bulk, J. Phys. Chem. B 110 (2006) 927–935.
[39] W.F. Zhang, Y.L. He, M.S. Zhang, Z. Yin, Q. Chen, Raman scattering study on anatase TiO_2 nanocrystals, J. Phys. D: Appl. Phys. J 33 (2000) 912–916.
[40] J.L. Li, X.T. Xu, X.J. Liu, W. Qin, L.K. Pan, Novel cake-like N-doped anatase/rutile mixed phase TiO_2 derived from metal-organic frameworks for visible light

photocatalysis, Ceram. Int. 43 (2017) 835–840.
[41] L. Zeng, Z. Lu, M.H. Li, J. Yang, W.L. Song, D.W. Zeng, C.S. Xie, A modular calcination method to prepare modified N-doped TiO_2 nanoparticle with high photocatalytic activity, Appl. Catal. B: Environ. 183 (2016) 308–316.
[42] A. Enrique, R. Garcia, Y.P. Sun, K.R. Gil, D. Raftery, ^{15}N solid state NMR and EPR characterization of N-doped TiO_2 photocatalysts, J. Phys. Chem. C 111 (2007) 2738–2748.
[43] J.M. Coronado, A.J. Maira, J.C. Conesa, K.L. Yeung, V. Augugliaro, J. Soria, EPR study of the surface characteristics of nanostructured TiO_2 under UV irradiation, Langmuir 17 (2001) 5368–5374.
[44] M.A. Centeno, M. Paulis, M. Montes, J.A. Odriozola, Catalytic combustion of volatile organic compounds on gold/titanium oxynitride catalysts, Appl. Catal. B: Environ. 61 (2005) 177–183.
[45] M. Sathish, B. Viswanatha, R.P. Viswanath, C.S. Gopinath, Synthesis, Characterization, electronic structure, and photocatalytic activity of nitrogen-doped TiO_2 nanocatalyst, Chem. Mater. 17 (2005) 6349–6353.
[46] H. Han, R.B. Bai, Buoyant, photocatalyst with greatly enhanced visible-light activity prepared through a low temperature hydrothermal method, Ind. Eng. Chem. Res. 48 (2009) 2891–2898.
[47] A. Ishikawa, T. Takata, J.N. Kondo, M. Hara, H. Kobayashi, K. Domen, Oxysulfide $Sm_2Ti_2S_2O_5$ as a stable photocatalyst for water oxidation and reduction under visible light irradiation ($\lambda \leq 650$ nm), J. Am. Chem. Soc. 124 (2002) 13547–13553.
[48] F.F. Santiago, G.G. Belmonte, J. Bisquert, P. Bogdanoffband, A. Zabanc, Mott-schottky analysis of nanoporous semiconductor electrodes in dielectric state deposited on SnO_2(F) conducting substrates, J. Electrochem. Soc. 150 (2003) 293–298.
[49] W. Dai, X. Wang, P. Liu, Y. Xu, G. Li, X. Fu, Effects of Electron transfer between TiO_2 films and conducting substrates on the photocatalytic oxidation of organic pollutants, J. Phys. Chem. B 110 (2006) 13470–13476.
[50] M. Jakob, H. Levanon, Charge distribution between UV-irradiated TiO_2 and gold nanoparticles: determination of shift in the fermi level, Nano Lett. 3 (2003) 353–358.
[51] V. Subramanian, E.E. Wolf, P.V. Kamat, Catalysis with TiO_2/Gold nanocomposites effect of metal particle size on the fermi level equilibratio, J. Am. Chem. Soc. 126 (2004) 4943-495.
[52] T. Berger, J.A. Anta, V. Morales-Flórez, Electrons in the band gap: spectroscopic characterization of anatase TiO2 nanocrystal electrodes under fermi level control, J. Phys. Chem. C 116 (2012) 11444–11455.
[53] L. Jing, X. Sun, B. Xin, B. Wang, W. Cai, H. Fu, The preparation and characterization of La doped TiO2 nanoparticles and their photocatalytic activity, J. Solid State Chem. 177 (2004) 3375–3382.
[54] A.J.E. Rettie, K.C. Klavetter, J.F. Lin, A. Dolocan, H. Celio, A. Ishiekwene, H.L. Bolton, K.N. Pearson, N.T. Hahn, C.B. Mullins, Improved visible light harvesting of WO_3 by incorporation of sulfuror iodine: a tale of two impurities, Chem. Mater. 26 (2014) 1670–1677.
[55] P. Madhusudan, J.R. Ran, J. Zhang, J.G. Yu, G. Liu, Novel urea assisted hydrothermal synthesis of hierarchical $BiVO_4/Bi_2O_2CO_3$ nanocomposites with enhanced visible-light photocatalytic activity, Appl. Catal. B: Environ. 110 (2011) 286–295.
[56] D.N. Ke, T.Y. Peng, L. Ma, P. Cai, P. Jiang, Photocatalyt -ic water splitting for O_2 production under visible-light irradiation on $BiVO_4$ nanoparticles in different sacrificial reagent solutions, Appl. Catal. A Gen. 350 (2008) 111–117.
[57] Z. Zhang, X. Wang, J. Long, Q. Gu, Z. Ding, X. Fu, Nitrogen-doped titanium dioxide visible light photocatalyst: spectroscopic identification of photoactive centers, J. Catal. 276 (2010) 201–214.